Disturbances and Eddy Fluxes in Southern Hemisphere Flows: Linear Theory

J. S. FREDERIKSEN[1]

National Center for Atmospheric Research,[2] Boulder, CO 80307

(Manuscript received 30 June 1980, in final form 12 December 1980)

ABSTRACT

The instability characteristics of Southern Hemisphere zonally averaged flows are studied for January, May and August basic states in a spherical, inviscid, adiabatic, quasi-geostrophic multilevel model. The growing disturbances may have considerably more complex growth rate curves, structures and momentum and heat fluxes than found for idealized single jet and Northern Hemisphere flows. For August, the largest growth rate occurs at the largest zonal wavenumber studied ($m = 16$), while for January and May it occurs at a more conventional intermediate value ($m = 10$). The modes for January have many properties in common with modes found with idealized single jet basic states, but in addition to eastward-propagating disturbances long-wave westward propagating disturbances occur. For May and August, the presence of both the subtropical and polar jets is felt by the eastward-propagating disturbances. Some of these grow primarily on one jet or the other, while other modes have two maxima of the disturbance streamfunctions at latitudes near the two jet streams. The presence of the two jets may also result in more complex momentum fluxes than found previously.

For each month, appropriate modes do have maximum streamfunction amplitude and eddy fluxes at the correct latitudes, but the usual vertical structure problem of linear theory occurs, *viz.*, the amplitudes of streamfunctions, momentum and heat fluxes are too large at the surface compared with at the tropopause in relation to observations. However, for May, the instability results appear to contradict the usual hypothesis of baroclinic instability theory that one of the members, lying on the growth rate curve, as a function of zonal wavenumber, with largest growth rates, should be of the most meteorological significance. In fact, the second fastest growing modes of intermediate zonal wavenumbers appear to correspond most closely with observations, emphasizing the importance of finding all the growing modes by using, for example, an eigenvalue approach.

1. Introduction

Baroclinic instability studies carried out with multilevel models incorporating spherical geometry and zonal flow basic states (Gall, 1976a,b; Simmons and Hoskins, 1976, 1977; Frederiksen, 1978b) have led to new insights into the usefulness and limitations of linear theory in explaining observed disturbance amplitudes and fluxes. Although β-plane calculations have increased our understanding of atmospheric dynamics, a quantitative comparison of observations and theory requires the incorporation of the correct geometry, particularly for sensitive quantities such as eddy momentum fluxes. In fact, β-plane studies may lead to spurious results for both linear (Stone, 1969) and nonlinear (Frederiksen and Sawford, 1980) flow problems.

Recently, the instability of more general basic states having zonal as well as meridional and vertical variations has been studied in spherical two-layer models (Frederiksen, 1978a, 1979a, 1980) and in multilevel models (Frederiksen, 1979b). In the Northern Hemisphere where there are large variations with longitude of the zonal wind, with jet stream maxima off the east coasts of America and Japan, it is particularly important to use basic states with fully three-dimensional variations. Indeed, a two-layer spherical model incorporating the gross stationary planetary wave structure of Northern Hemisphere winter flow (Frederiksen, 1979a) was able to capture the essential features of the observed regions of preferential cyclogenesis and the localized nature of band-pass time-filtered eddy momentum and heat fluxes as derived from observations by Blackmon *et al.* (1977).

In the Southern Hemisphere, the flow is considerably more zonal; thus the use of zonally averaged basic states might be expected to be more reasonable. Thus in the present initial study of disturbances and eddy fluxes produced with Southern Hemisphere basic flows, we shall restrict our attention to zonally averaged states. The instability of July Southern Hemisphere flow on a sphere to long waves of zonal wavenumbers 2–5 which extend into the stratosphere has recently been considered by Hartmann (1979) using an initial value approach in a simplified quasi-geostrophic model. Here we are primarily interested

[1] On leave from CSIRO, Division of Atmospheric Physics, Aspendale, Victoria, Australia 3195.

[2] The National Center for Atmospheric Research is sponsored by the National Science Foundation.

0022-4928/81/040673-17$08.25

TABLE 1. The normalized pressure levels at which the streamfunction is evaluated.

σ
0.009
0.074
0.189
0.336
0.500
0.664
0.811
0.926
0.991

in studying the instability of zonal flows for different months (January, May and August) to growing tropospheric modes of widely varying zonal scales in a spherical multilevel quasi-geostrophic (QG) model originally proposed by Lorenz (1960). We use an eigenvalue approach which yields the growth rates and structures of all the growing modes at a given zonal wavenumber. This turns out to be important, particularly for the May and August flows when both the subtropical and polar jets play a crucial role in the stability.

In Section 2 we summarize the equations defining the multilevel QG model and in Section 3 we present the basic states for January, May and August. For each of these months, growth rates and phase speeds of all the growing modes as functions of zonal wavenumber are examined in Section 4. In Sections 5, 6 and 7 we examine the structure and eddy momentum and heat fluxes of some of the growing modes for each of the three months. The conclusions of this work are presented in Section 8.

2. The quasi-geostrophic equations

For this study we use the same inviscid, adiabatic, QG spherical equations as were employed in Frederiksen (1978b) and originally derived by Lorenz (1960). With a continuous vertical representation, these equations may be written in pressure coordinates in the form

$$\frac{\partial \nabla^2\psi}{\partial t} = -J(\psi, \nabla^2\psi + f) - \nabla\cdot(f\nabla\chi), \quad (2.1)$$

$$\frac{\partial T}{\partial t} = -J(\psi, T) + \Sigma w, \quad (2.2)$$

$$\frac{\partial \Phi}{\partial p} = -\frac{RT}{p}, \quad (2.3)$$

$$\nabla^2\Phi = \nabla\cdot(f\nabla\psi), \quad (2.4)$$

$$-\frac{\partial w}{\partial p} = \nabla^2\chi, \quad (2.5)$$

$$f = 2\Omega\mu, \quad (2.6)$$

$$\Sigma = -\left(\frac{\partial \bar{\bar{T}}}{\partial p} - \kappa\frac{\bar{\bar{T}}}{p}\right). \quad (2.7)$$

In these equations, ψ is the streamfunction, χ the velocity potential, T the temperature, Σ the static stability parameter, $w = dp/dt$, the "vertical" velocity, Φ the geopotential height, R the gas constant for air, f the Coriolis parameter, κ the ratio of the gas constant to the specific heat of air at constant pressure, $\bar{\bar{T}}$ the horizontally averaged temperature, p the pressure and μ = sin(latitude).

In the present study, we employ a multilevel version of the above QG equations, and details of the finite differencing of the equations in the vertical are given in Frederiksen (1978b). As discussed there, the streamfunctions and temperatures are specified at alternate full and half levels. For the present study, we use a nine-level model in which the streamfunctions are specified at the normalized pressure levels shown in Table 1. Here σ = p/1000 is the normalized pressure since topographic effects will not be considered in this article. The temperatures are evaluated at half levels taken halfway between adjacent levels given in Table 1. The levels shown in Table 1 have been chosen to correspond to those generally used for Southern Hemisphere forecasts using the Australian spectral model developed by Bourke *et al.* (1977). This will facilitate a subsequent comparison of the present linear study with nonlinear integrations carried out with this model (Frederiksen, 1981). In common with most previous studies of tropospheric disturbances, the resolution of the stratosphere is poor. Nonetheless, it is felt that this should not change greatly the character of the tropospheric disturbances of interest here.

The method of linearizing the multilevel equations about a basic state of zonal flow and formulating the eigenvalue problem for the complex frequency $\omega = \omega_r + i\omega_i$ and the corresponding spectral amplitudes of the perturbation growing on the zonal flow is given in Appendix A of Frederiksen (1978b).

3. Basic zonal flow states

For the basic states, we have taken the Southern Hemisphere flows (symmetrized about the equator) characteristic of January, May and August; the zonal flows for these months are shown in Fig. 1.[3] These diagrams were obtained by fitting cubic splines to values of the zonal wind given at the σ levels shown in Table 1. The January basic state was obtained from monthly averages from 1972 to 1976 as determined by the Australian Weather Bureau analysis. The May and August states are "instantaneous" values obtained for 19 May 1979 and 23 August 1975.

[3] Throughout this article we use latitude to mean south latitude; positive eddy fluxes are toward the South Pole and negative fluxes are equatorward.

The May field was obtained during the First GARP Global Experiment (FGGE) special observing period and as such is probably as accurate as one is likely to obtain in the Southern Hemisphere. For the August field, the values at the σ levels in Table 1 above 100 mb have been chosen to represent approximate climatology. We notice that the zonal wind fields shown in Fig. 1 are in close qualitative agreement with those given in Fig. 3.13 of Newell *et al.* (1972) and in Figs. 19 and 20 of Knittel (1976), although the three monthly averages in Newell *et al.* are somewhat less intense as might be expected.

Fig. 2 shows the vertical profile of the horizontally averaged temperature for each of the three months from which the static stability parameter may be derived through Eq. (2.7).

4. Growth rates and phase speeds

Figs. 3, 4 and 5 show for January, May and August the growth rates and phase speeds of perturbations having the general form

$$f = \mathrm{Re}\{\sum_{n=|m|}^{|m|+J} f_{mn} P_n^m(\mu) \exp[i(m\lambda - \omega t)]\}, \quad (4.1)$$

where $\omega = \omega_r + i\omega_i$ and ω_i is the growth rate and ω_r/m the phase speed. In Eq. (4.1), f is any of the fields in Eqs. (2.1)–(2.7) at a given vertical level, f_{mn} are spectral amplitudes, and $P_n^m(\mu)$ are associated orthonormal Legendre functions. Throughout this article we use the standard mathematical nomenclature with m [replacing the k used in Frederiksen (1978b)] the zonal wavenumber and n the total wavenumber. We shall only be concerned with the even disturbance modes (antisymmetric streamfunctions) for which the total wavenumber then takes the values $n = m + 1, m + 3, \ldots, m + J$, where we choose the truncation wavenumber $J = 25$.

As mentioned in Frederiksen (1978b), the eigenvalue method employed here allows one to calculate all the growing modes without convergence problems for a given spatial resolution. Thus in Figs. 3–5 we have shown as many of the growth rates and phase speeds as are conveniently depicted. For the relatively simple January flow characterized by a single jet, the growth rate and phase speed curves bear some similarity to the idealized 30° jet studied in Frederiksen (1978b) (Fig. 1). In particular, the phase speeds are practically constant with changing zonal wavenumber, and the fastest growing mode has zonal wavenumber $m = 10$. In contrast to the purely eastward-propagating waves for the 30° jet, for the present January flow there are also westward-propagating waves which, for the modes shown in the curve H, are the fastest growing for zonal wavenumbers 1–5. As we shall see in the next section, these waves appear to propagate in the westward basic zonal wind in the lower troposphere near 70 and 80° and in the stratosphere.

For the two flows with the double jet structure, there are some modes with almost constant phase speed with changing zonal wavenumber m and as well modes for which the phase speed changes with m (generally decreasing). For May the maximum growth rate attained is considerably larger than for either January or August. We further note that the phase speed curve for modes A for May is decreasing with increasing zonal wavenumber m, while for January and August phase speed curves A are practically constant. In contrast, modes B for May have constant phase speed and maximum growth rate similar to those for modes A for January and August. Thus one might expect that modes A for May are fundamentally different from those for January and August as we shall confirm in the following sections.

For August we see that the fastest growing mode displayed occurs at the largest zonal wavenumber studied, *viz.*, $m = 16$. Gall (1976a,b) has previously noted that for a particular Northern Hemisphere flow and for an idealized jet the fastest growing modes also occurred at unrealistically short wavelengths compared with observations. It is interesting that here non-geostrophic effects are not necessary to move the growth rate of the fastest growing mode to large zonal wavenumber (cf. Frederiksen, 1978b).

5. Disturbances and eddy fluxes for January

Here and in the following two sections, we study the disturbances and eddy fluxes for the different months. For convenience in comparing the results, we consider first January, then August and finally May.

It is perhaps useful to summarize some of the problems encountered when comparing linear instability results with observations and to introduce a shorthand notation for referring to these problems and concepts in the following sections.

a. The vertical structure problem

It has been found in previous β-plane and spherical geometry studies (Green, 1970; Gall, 1976a; Simmons and Hoskins, 1977; Frederiksen, 1979b) that linear instability solutions with purely zonal basic states generally have too large amplitude near the surface relative to that at the tropopause. This problem occurs for each of the perturbation quantities studied here, *viz.*, streamfunctions, temperatures, and horizontal eddy momentum and heat fluxes. Nevertheless, in most cases linear theory does seem to predict correctly the latitude at which the largest amplitudes of the streamfunctions, temperatures and eddy fluxes occur.

b. The nonlinear analog mode

Comparisons between observations and nonlinear integrations starting with zonal flows plus small per-

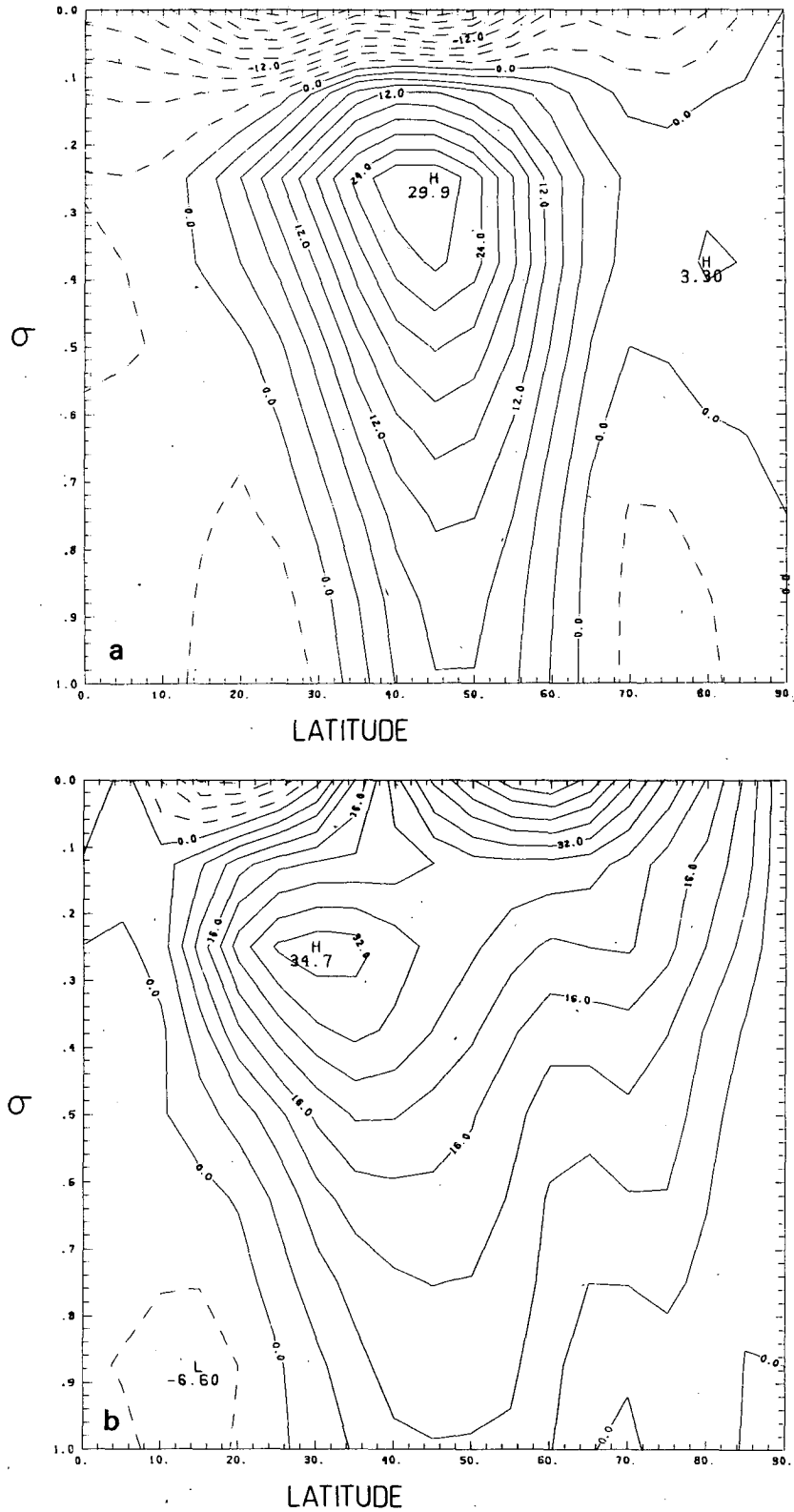

FIG. 1. Meridional cross sections of basic state zonal winds as a function of normalized pressure σ and (south) latitude for (a) January, (b) May and (c) August. The method used to construct these diagrams is described in the text.

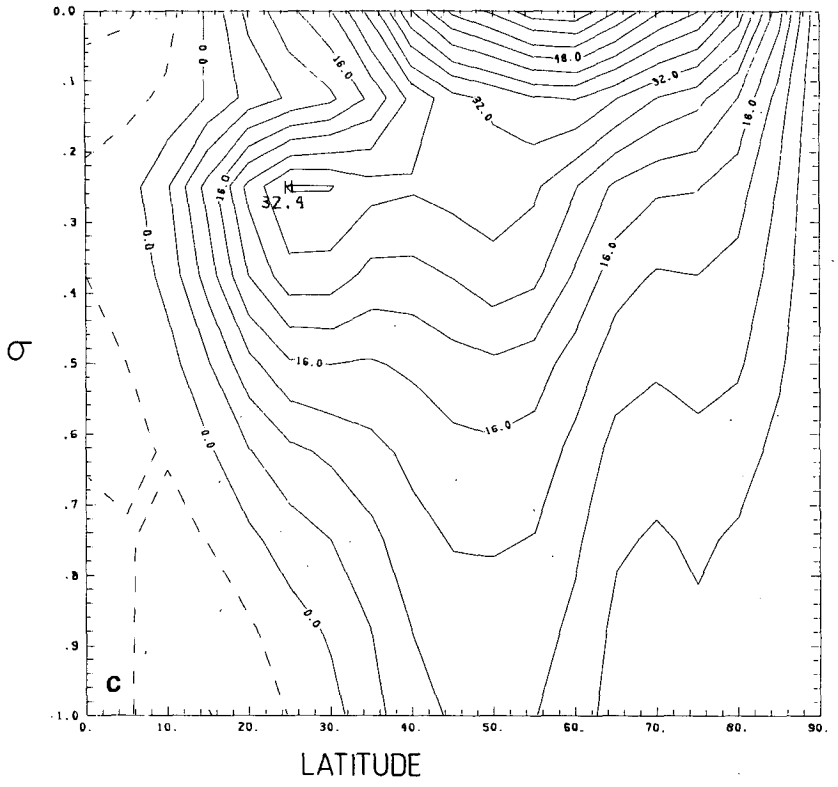

FIG. 1c.

turbations also have been carried out in spherical geometry (Gall, 1976b; Simmons and Hoskins, 1978). As the perturbations approach their maximum amplitudes, growth ceases near the surface but continues aloft near the tropopause. Thus an average of the perturbation quantities, taken over the growing, occluding and decaying phases, yields considerably better comparison with observations. In the following sections, we shall also discuss how the linear results might be modified if one started a nonlinear integration with a given zonal flow and a perturbation amplitude, denoted A, say, of given zonal wavenumber, obtained from linear instability theory. We shall call the resulting nonlinear perturbation the nonlinear analog of A.

1) DISTURBANCE STREAMFUNCTIONS AND TEMPERATURES

Figs. 6a and 6b show the amplitudes of the disturbance streamfunction and temperature for the fastest growing eastward propagating mode (A) with zonal wavenumber $m = 10$. As in the early β-plane studies (Charney, 1947; Eady, 1949) and in spherical studies with idealized jets (Simmons and Hoskins, 1976; Frederiksen, 1979b), the streamfunction exhibits a slight westward phase tilt with height (not shown). The disturbance streamfunction maximum occurs slightly poleward of the jet-stream maximum which is consistent with two-layer spherical results (see, e.g., Baines and Frederiksen, 1978). The streamfunctions and temperatures also were studied for $m = 7$; for this case the qualitative appearances are similar to those for $m = 10$ except that, as expected, there is a relative increase in the upper level amplitudes.

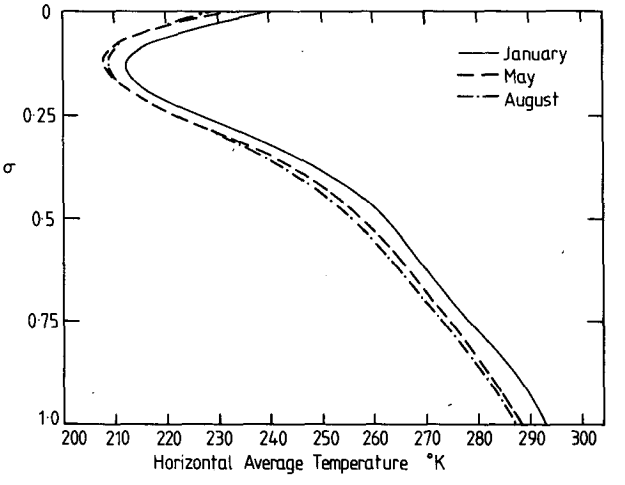

FIG. 2. Profiles of the horizontally averaged temperature as a function of normalized pressure σ for the three different months shown.

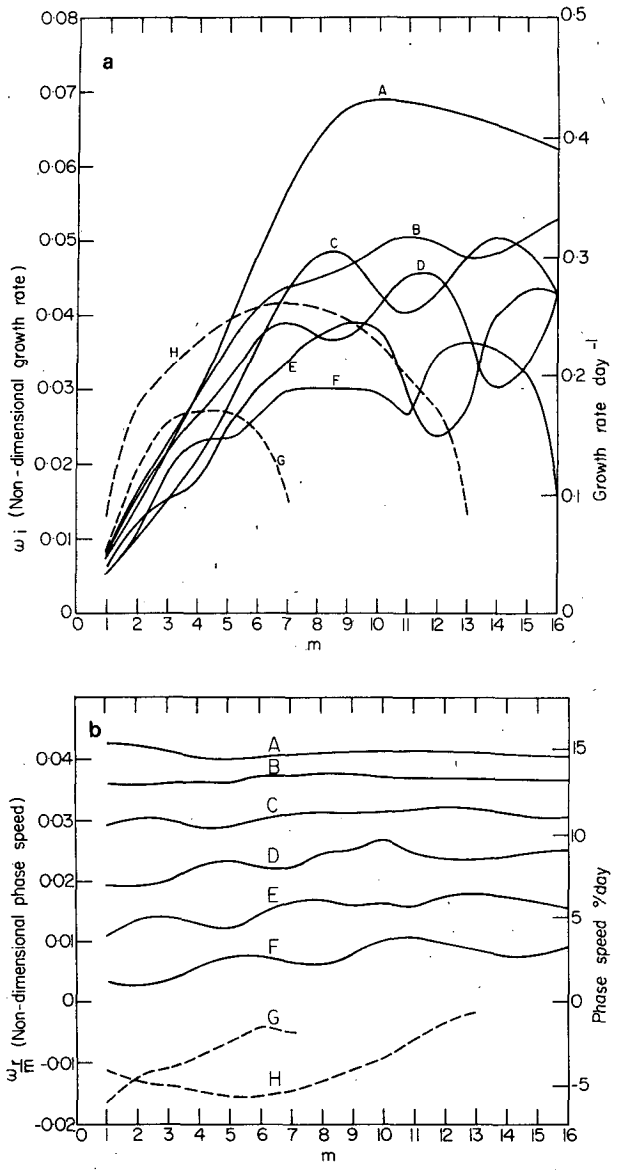

FIG. 3. Growth rates (a) and phase speeds (b) of some of the fastest-growing disturbance modes for January as a function of zonal wavenumber m. Since the spectra on a sphere are discrete, the lines joining the points in Fig. 1 are purely to aid visualization; they have been drawn in such a way that the lines joining the phase speeds have as few intersections as possible.

At zonal wavenumber $m = 4$, the fastest-growing perturbation (H) has a phase speed of approximately $-5°$ day^{-1}. This slowly westward-propagating mode has maximum streamfunction amplitude near 77° latitude as shown in Fig. 7. Thus this mode appears to be propagating in the westward basic flow that occurs in the lower troposphere between 70 and 80° latitude and in the stratosphere at these latitudes. In this case, the temperature perturbation amplitude is also centered at 77° latitude and has a maximum at 750 mb. This is also consistent with the tendency of longer waves to become unstable closer to the pole.

To see how well the instability theory results compare with observations, we compare the perturbation streamfunction amplitudes with the standard deviation of the meridional wind component shown in Table 3.6 of Newell *et al.* (1972). The largest observed deviations do indeed occur near 50° latitude for the period December–February, in agreement with the location of maximum perturbation amplitude for the fastest growing mode (A at $m = 10$). However, for both this mode and for the mode A at $m = 7$, the usual vertical structure problem discussed above occurs. The observations also show quite substantial deviations of the meridional wind as far south as 80° latitude. Thus it may be that the nonlinear analog of the mode H, at $m = 4$, say (for which one would expect largest amplitude near the tropopause toward the end of the growth period), could contribute to the standard deviation of the meridional wind at these polar latitudes. The phase speed of mode H, of course, may be affected by inclusion of topographic, viscous and nonlinear effects.

2) EDDY MOMENTUM FLUXES

Fig. 8 shows the zonally averaged eddy momentum flux for mode A in Fig. 3 with $m = 10$. The momentum flux is largely poleward (positive) with a maximum in the lower troposphere and a secondary maximum at 700 mb; there is only a weak equatorward (negative) flux in the lower troposphere. For zonal wavenumber $m = 7$, the momentum flux for mode A is qualitatively similar but with a relative increase in the poleward flux in the upper troposphere and into the stratosphere and the secondary maximum being raised to 600 mb. In addition, there is an increase in the equatorward flux in the lower troposphere and the apperance of a region of equatorward flux centered on 300 mb and at latitude 56°. In both cases the flux of momentum tends to be into the jet stream maximum but centered somewhat poleward of it. This is consistent with two-layer results (Baines and Frederiksen, 1978; Frederiksen, 1980a) where the general character of momentum fluxes may be related to general stability criteria. We note that the fluxes are qualitatively similar to those for the 39° jet studied in the two-layer model of Baines and Frederiksen (1978).

Comparing these results with those shown in Fig. 4.9 of Newell *et al.* (1972) for December–February, we see first that the usual vertical structure problem occurs. In addition, the present linear results do not show equatorward fluxes with maxima centered on 70° latitude as found in the observations. It is interesting that the modes H in Fig. 3, an example of which is shown in Fig. 7 for $m = 4$, do in fact produce largely equatorward momentum fluxes (not

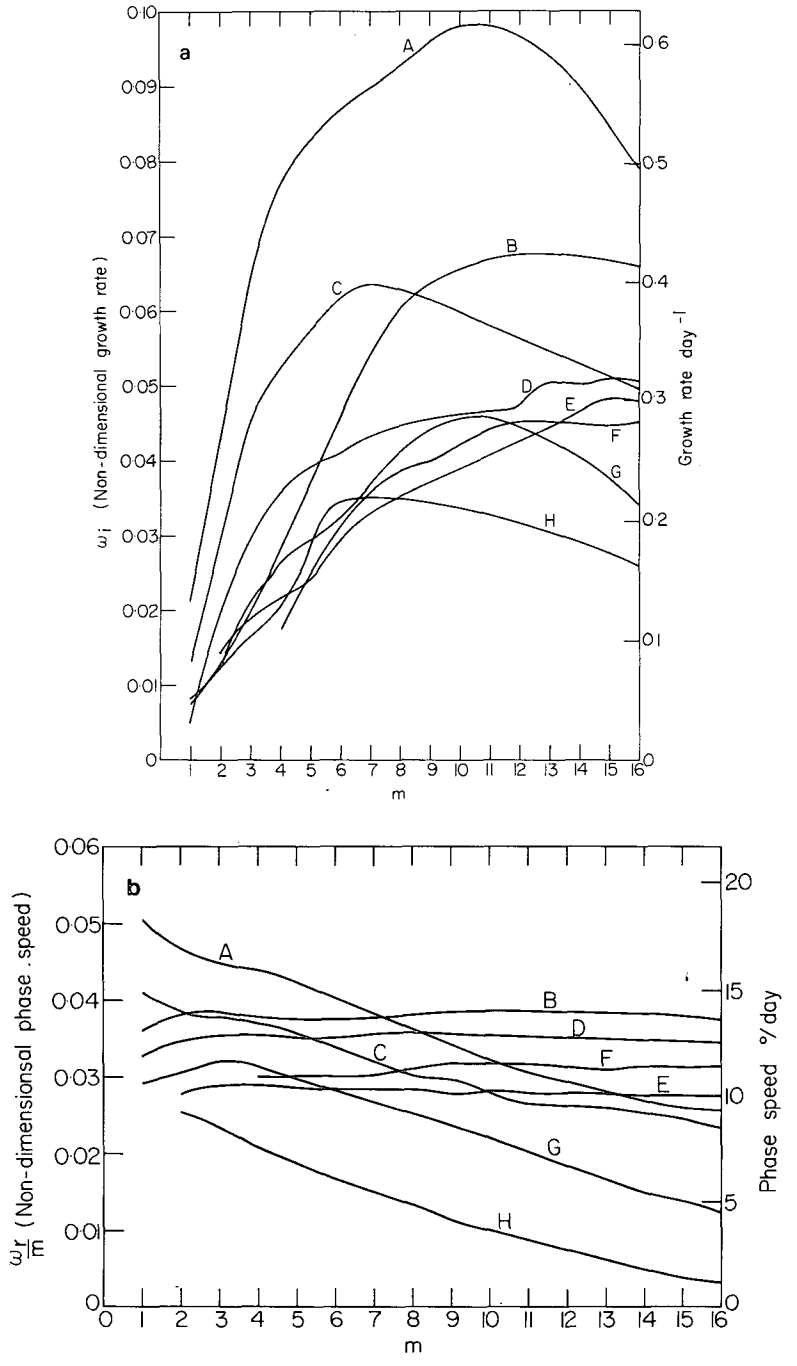

FIG. 4. As in Fig. 3 for May.

shown) centered near latitude 70° and having considerable amplitude throughout most of the troposphere (as expected, the low-level fluxes are again too large).

3) EDDY HEAT FLUXES

Fig. 9 shows the zonally averaged eddy heat flux at $m = 10$ for mode A in Fig. 3. The flux is practically purely poleward and confined to the lower troposphere with a maximum centered on 50° latitude. For mode A at $m = 7$, the qualitative appearance of the heat flux is similar to that in Fig. 9 but it extends farther into the troposphere. The heat fluxes do not depend on the subtle phase differences between the streamfunction and its latitudinal derivative (as do the momentum fluxes) but, in general, are rather similar to the streamfunction amplitudes squared and are directed poleward.

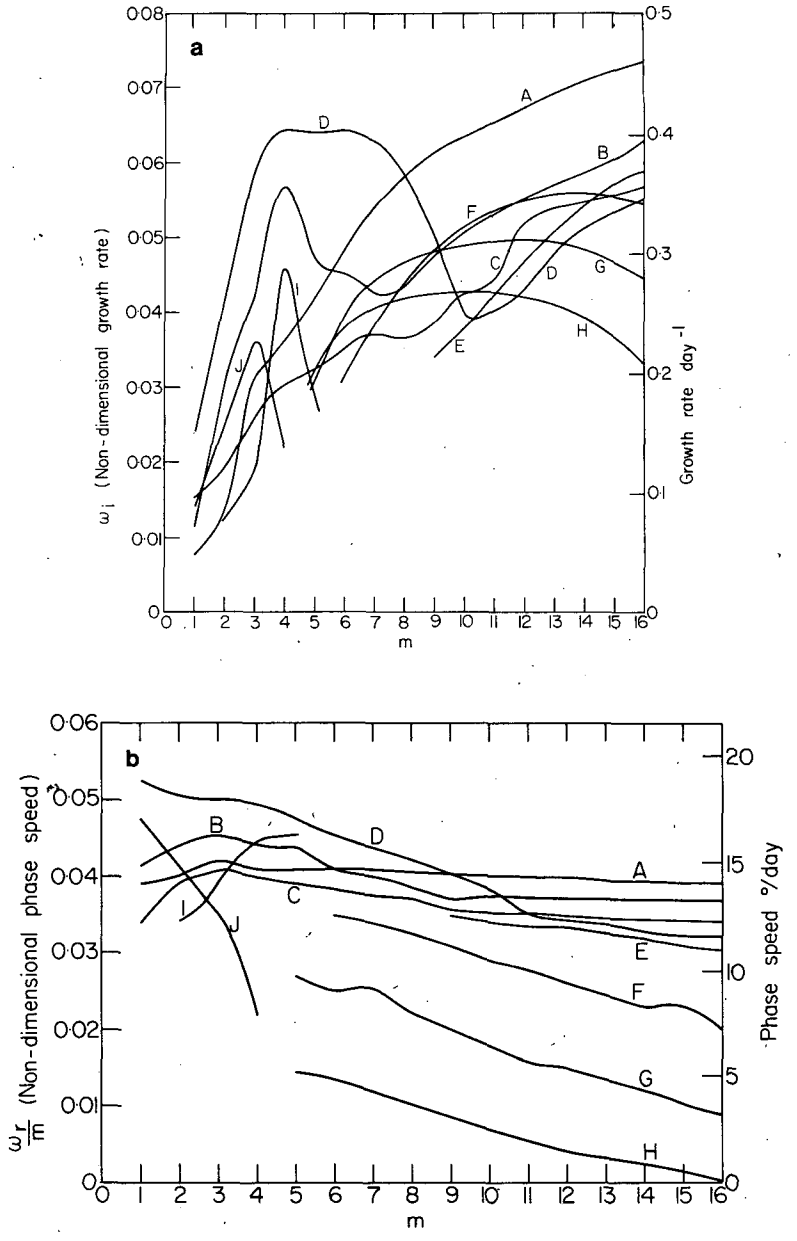

FIG. 5. As in Fig. 3 for August.

Comparing Table 7.2 of Newell *et al.* (1974), which shows the total eddy heat transport averged for December to February, with the above results, we see that at least linear theory predicts the correct approximate latitude of maximum poleward heat flux (notice the different sign convention in Newell *et al.*). The latitudinal spread, however, is somewhat larger in the observations; this may be partly due to averaging over a number of different months and years and to a broadening produced in the nonlinear regime. It also may be due to modes like that shown in Fig. 7 for which the heat flux is again practically purely poleward but is centered at 750 mb and 76° latitude. We note further that the maximum occurring at 200 mb in the observations does not appear in the linear results. van Loon (1980), using the recent FGGE data for January 1979, obtains only a maximum poleward heat flux of ~2°C m s^{-1} at 200 mb compared with Newell *et al.*'s value of 17.6°C m s^{-1}. There appear to be considerable difficulties in calculating heat fluxes for the Southern Hemisphere. Australian operational analyses before FGGE show

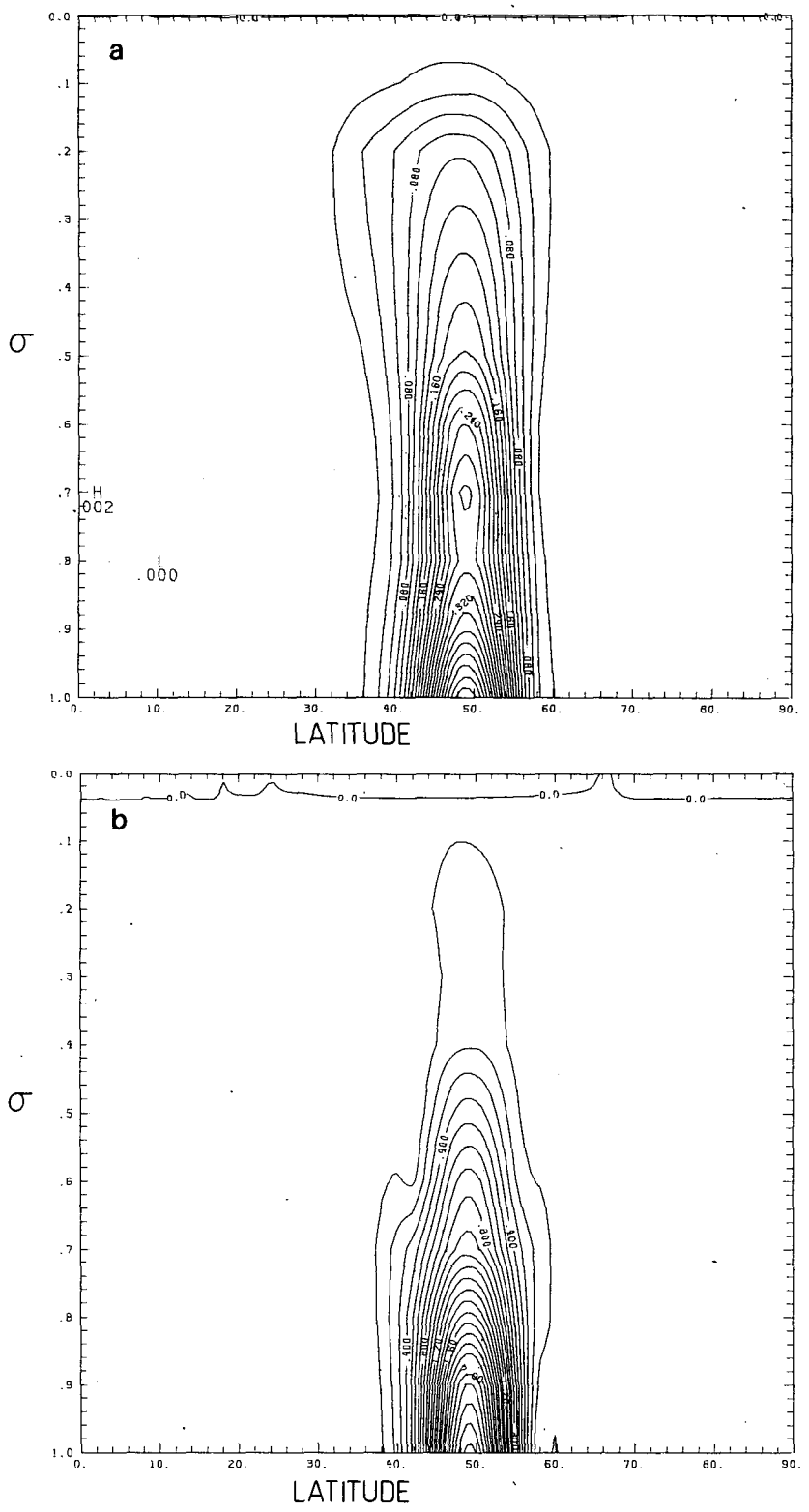

FIG. 6. Disturbance streamfunction (a) and temperature (b) amplitudes for the fastest growing perturbation (A with zonal wavenumber $m = 10$), with the January basic state, as a function of normalized pressure σ and (south) latitude. The normalizations of the amplitudes are arbitrary.

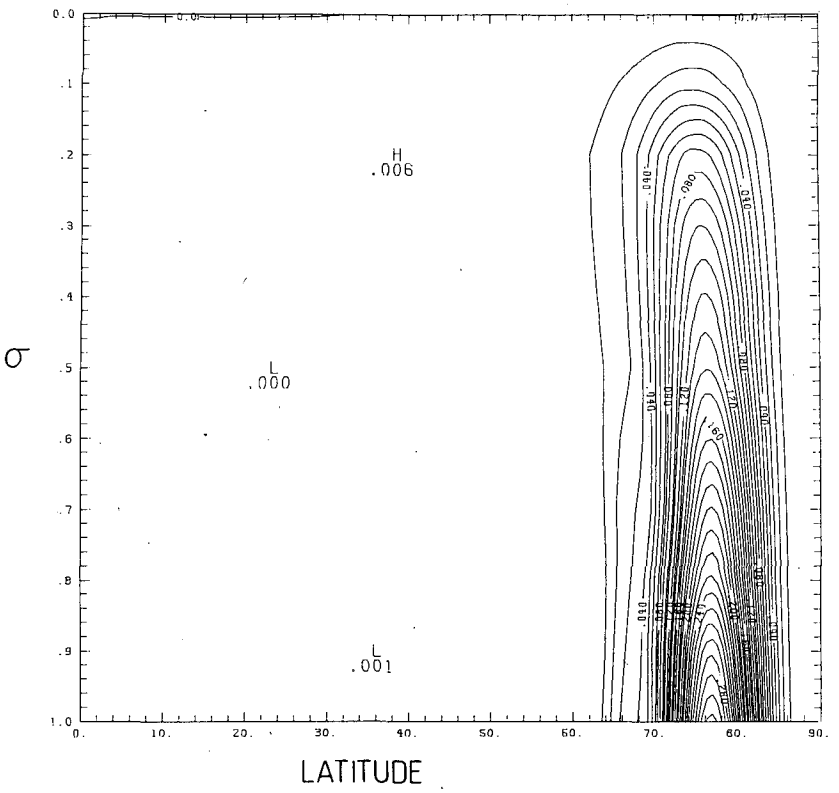

FIG. 7. Disturbance streamfunction amplitude for the fastest growing perturbation with zonal wavenumber $m = 4$ (H), with the January basic state, as a function of normalized pressure σ and (south) latitude.

an equatorward flux at and above 200 mb, although van Loon argues by comparison with individual station data that this result is anomalous.

6. Disturbances and eddy fluxes for August

For the remainder of this article, we shall concentrate on the new aspects of the baroclinic instability results introduced by the presence of two jets in the basic state.

a. Disturbance streamfunctions

We notice from Fig. 5 that, at zonal wavenumber $m = 8$, the fastest growing eastward propagating mode D and the second fastest growing eastward propagating mode A have practically identical growth rates and similar phase speeds. Such modes would be difficult to separate had a time-stepping initial value approach been adopted rather than the present eigenvalue formulation. It is also interesting that the difficulty of initial value approaches in separating the fastest and second-fastest modes may occur not only for small zonal wavenumbers (cf. Simmons and Hoskins, 1976; Frederiksen, 1978b) but even at intermediate zonal wavenumbers.

The modes A and D at $m = 8$ are characteristic in many important aspects of these respective modes at other values of m. For this reason, we show in Figs. 10a and 10b the corresponding streamfunction amplitudes. While the second fastest growing mode A is largely growing on the subtropical jet with maximum amplitude at 50° latitude, it also has a small secondary maximum at 70° latitude indicating that it is also feeling the presence of the polar jet. In contrast, the fastest growing mode D has maximum amplitude at 70° latitude growing mainly on the polar jet and a secondary weak maximum at 50° latitude. As in two-layer model studies (e.g., Baines and Frederiksen, 1978), we see that the half-width of the amplitude decreases as the peak moves poleward.

At $m = 10$, mode A is qualitatively similar to that shown in Fig. 10a but has less latitudinal spread and less penetration into the upper troposphere and stratosphere, and the effect of the polar jet is practically absent in the streamfunction structure. Similarly, for mode D at $m = 7$ and 4, the streamfunction amplitudes are centered on latitude 70° as in Fig. 10b. For decreasing zonal wavenumber, we see an increased latitudinal spreading of the disturbance amplitude together with a relative increase in the upper

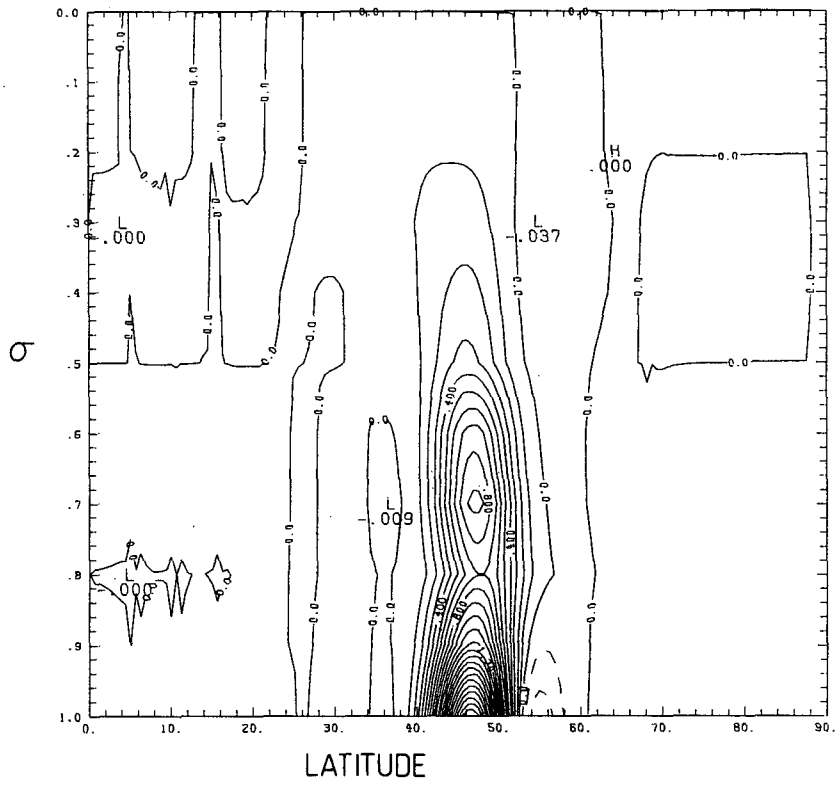

FIG. 8. Zonally averaged momentum flux $\overline{uv}$ for the disturbance shown in Fig. 6. The positive components (solid lines) are toward the South Pole and the negative (broken lines) are directed equatorward.

level amplitude, and the structure appears to be less influenced by the subtropical jet.

Comparing the above results with Table 3.6 of Newell *et al.* (1972) for the period June–August, we see that the vertical structure problem again occurs but that modes A correctly predict the latitude of largest standard deviation of the meridional wind. The latitudinal spread in the observations would be consistent with a broadening of modes A in the nonlinear regime or with having contributions from the nonlinear analogs of modes D.

b. Eddy momentum fluxes

For mode A at $m = 8$, the eddy momentum flux is very similar to that shown in Fig. 8, but with slightly reduced amplitude between 600 and 700 mb. At $m = 10$, the momentum flux is again similar to that in Fig. 8, but the relative upper level amplitudes are even further reduced.

The momentum fluxes associated with mode D exhibit considerable variability depending on the zonal wavenumber m, presumably reflecting the relative importance of the polar jet compared with the subtropical jet in determining disturbance quantities. For example, at $m = 8$ the momentum flux is largely confined below 500 mb, with poleward fluxes between 50 and 70° latitude and a narrow region of weaker equatorward flux centered on 46°. In contrast, at $m = 7$ the momentum flux is practically purely equatorward with largest amplitude at the lowest level and a secondary maximum at 650 mb. At $m = 4$, the momentum flux is largely poleward and confined between latitudes 50 and 70°; in this case, the flux also exhibits a secondary maximum at 200 mb with nearly one-half the value of the low-level maximum.

If we now look at the observed averaged eddy momentum fluxes for June–August, as shown in Fig. 4.9 of Newell *et al.* (1972), we see that for the Southern Hemisphere there are substantial poleward fluxes between latitudes 20 and 50° and equatorward fluxes centered on 70°. The maxima of both equatorward and poleward fluxes occur in the upper troposphere and, as discussed in Section 5, linear instability theory with purely zonal basic states seems incapable of capturing this aspect of the observations. We note that the poleward fluxes for mode A, discussed above, do occur in the right latitudinal band while the equatorward flux for mode D at $m = 7$ is centered on latitude 70°.

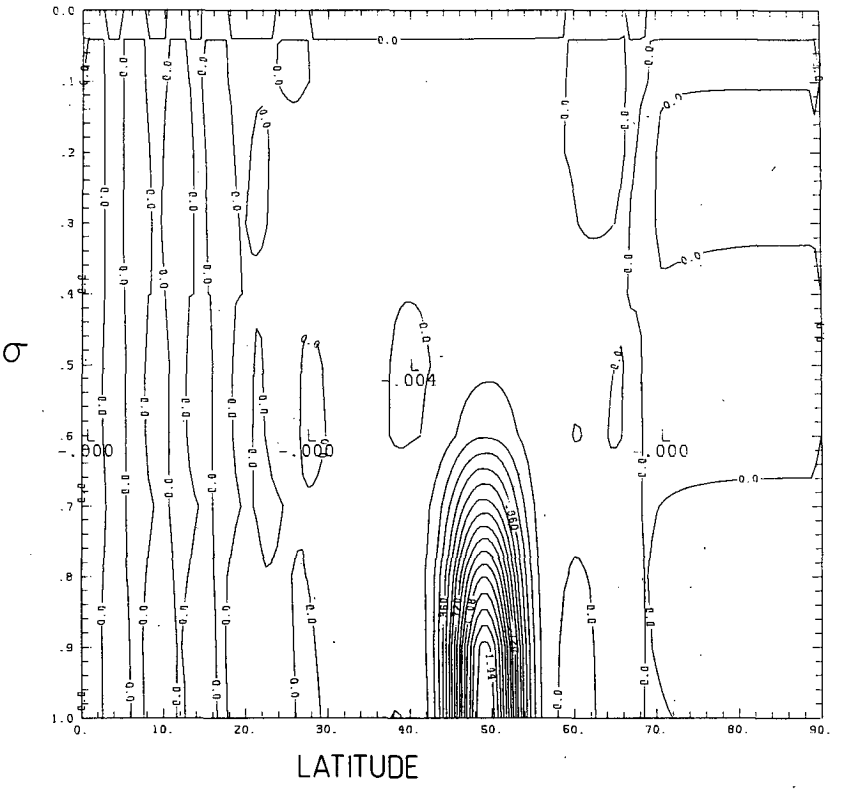

FIG. 9. Zonally averaged heat flux $\overline{vT}$ for the disturbance shown in Fig. 6.

c. Eddy heat fluxes

The poleward eddy heat fluxes for the different cases studied above are centered at the same latitudes as the corresponding disturbance steamfunctions and are confined to the lower stratosphere in a manner similar to that shown in Fig. 9. That is, for modes A discussed above, the heat fluxes have maximum amplitude in the lower troposphere at 50° latitude and for modes D at 70° latitude. Again the observations show the heat flux for June–August to be largest at the same latitude as it is for modes A.

7. Disturbances and eddy fluxes for May

a. Disturbance streamfunctions

Figs. 11a and 11b show the streamfunction amplitudes for the fastest (A in Fig. 4a) and second fastest (B) growing modes with zonal wavenumber $m = 10$ for the May basic state. Mode A is rather shallow and appears to be growing on the polar jet, but it also feels the presence of the subtropical jet as evidenced by the secondary maximum near 40° latitude. In contrast, mode B is somewhat deeper and is growing on the subtropical jet. It is interesting that mode A has a smaller meridional scale than mode B in contrast to the case of latitudinal uniform flow on a β-plane where the fastest growing mode has the largest meridional scale.

The structure of mode A also was examined at zonal wavenumbers $m = 5$ and 7. For these values, the streamfunction amplitude is again centered near 70° latitude with maximum amplitude in the lower troposphere and, as expected, increasing penetration into the upper atmosphere with decreasing wavenumber. For these cases the secondary maximum near 40° latitude does not occur.

Comparing these results with those for August, we see that the characteristics of mode A for May are similar to those for mode D for August, while mode B for May has, at $m = 10$, a structure very similar to that of mode A for August. Moreover, if we examine the variance of the observed meridional wind for March–May in Table 3.6 of Newell *et al.* (1972), which gives an indication of where the perturbation streamfunction should be largest, we see that for May, as for August and January, it occurs at latitude 50°. Thus, it appears that just as mode A (or rather the nonlinear analog of A) for August would be expected to be of most meteorological significance, so mode B should play this role for May. This appears to be a contradiction of the usual hypothesis of baroclinic instability theory that one of the members lying on the growth rate curve with

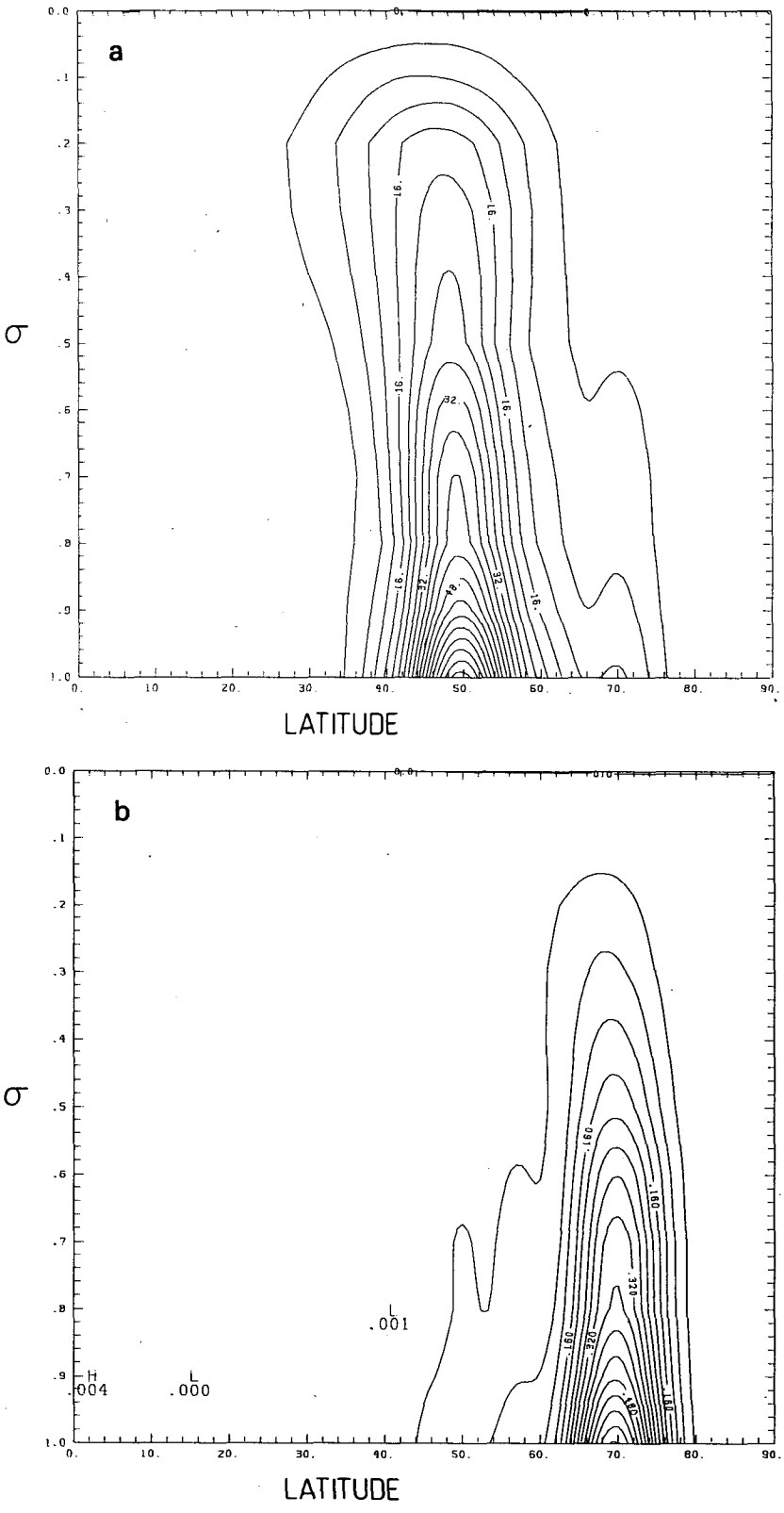

FIG. 10. Disturbance streamfunction amplitudes with zonal wavenumber $m = 8$ for the second fastest (a) (A) and fastest (b) (D) growing modes for the August basic state.

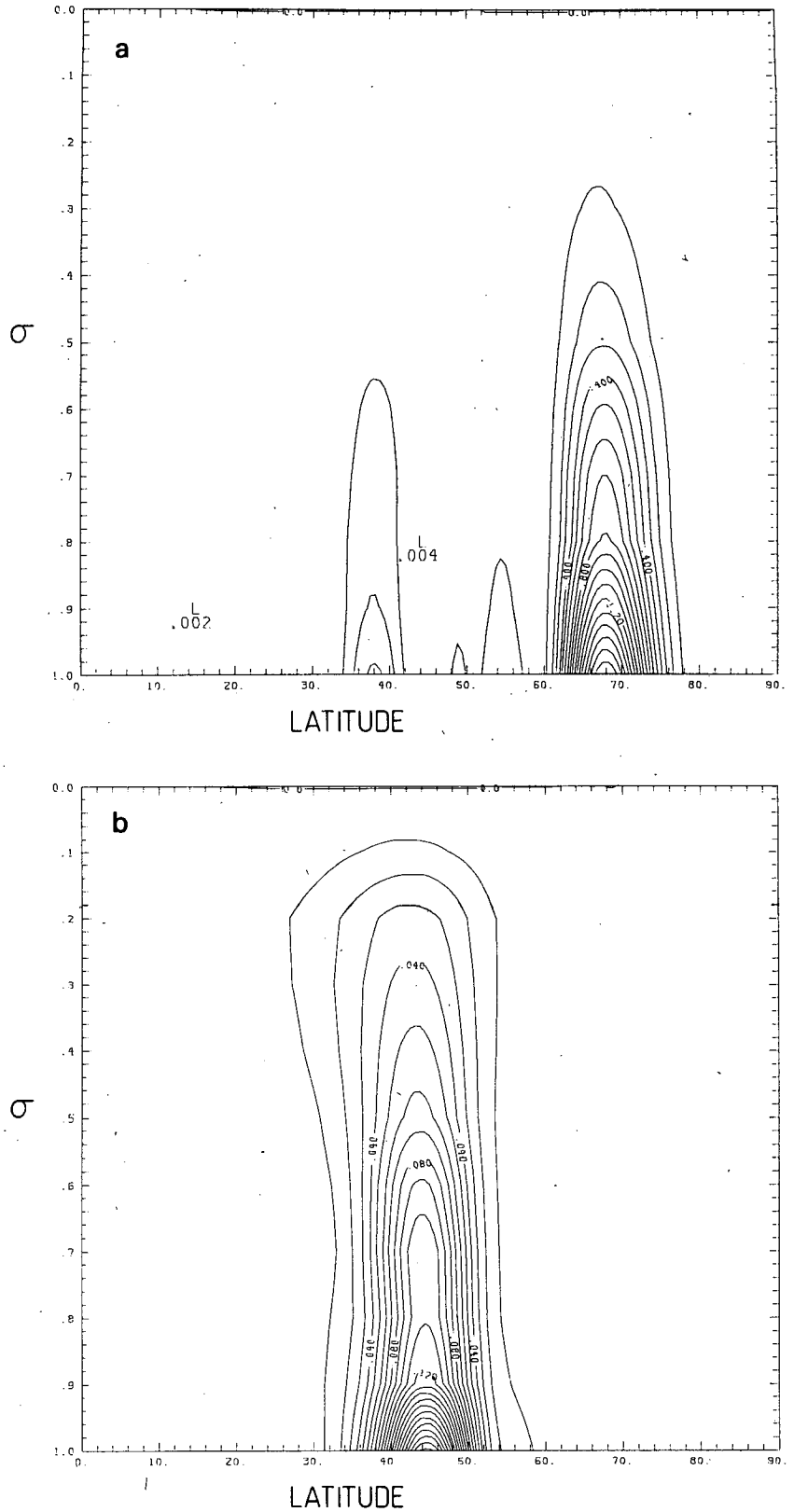

FIG. 11. Disturbance streamfunction amplitudes with zonal wavenumber $m = 10$ for the fastest (a) (A) and second fastest (b) (B) growing modes for the May basic state.

largest growth rates should be of most meteorological significance. Gall (1976a) noted that nonlinear effects may cause a decrease in the wavenumber of the wave with most meteorological significance compared with that predicted by baroclinic instability theory. This is due to the fact that the short waves, although faster growing in some cases than waves with intermediate wavenumbers, are not able to achieve the same amplitude and kinetic energy in the nonlinear regime. However, this appears to be the first time that a profile has been studied for which none of the fastest growing modes appears to correspond to those observed most frequently, but rather the meteorological significant modes have maximum amplitude at the same latitudes as those on the second fastest growth rate curve.

In a subsequent article (Frederiksen, 1980b), we study how nonlinear and viscous effects modify the fastest growing modes. We note that because mode A at $m = 10$ has a rather small spatial scale, being confined close to the pole, it might be that simply the introduction of viscosity would be sufficient to interchange the relative growth rates of A and B at $m = 10$. Because of the scale-selective nature of the normal viscosity parameterization, one would expect less effects on the larger scales corresponding to, say, $m = 5$ and 7. Thus one might expect viscosity to change curve A for May to look something like curve D for August. That is, while curve A would correspond to the most important long waves, curve B would represent the most important intermediate and short waves. It might also be thought that the inclusion of topography would stabilize modes A relative to modes B. However, this turns out not to be an important effect as shown in Frederiksen (1981).

b. *Eddy momentum fluxes*

Fig. 12 shows the eddy momentum flux for mode A at $m = 10$. Again, the complicated nature of the eddy momentum flux seems to be related to the fact that this mode is growing on both the subtropical and the polar jet. As for modes D for August, there is, for the present A modes, considerable variability of the momentum fluxes for different zonal wavenumbers. For example, at $m = 7$, the eddy momentum flux is practically purely equatorward, centered on 70° latitude and has significant amplitude throughout the troposphere.

For mode B at $m = 10$, the eddy momentum flux has again the same qualitative appearance and latitudinal location as shown in Fig. 8. In this case, the poleward fluxes in the middle troposphere are reduced compared to those shown in Fig. 8.

If we now examine the averaged Southern Hemi-

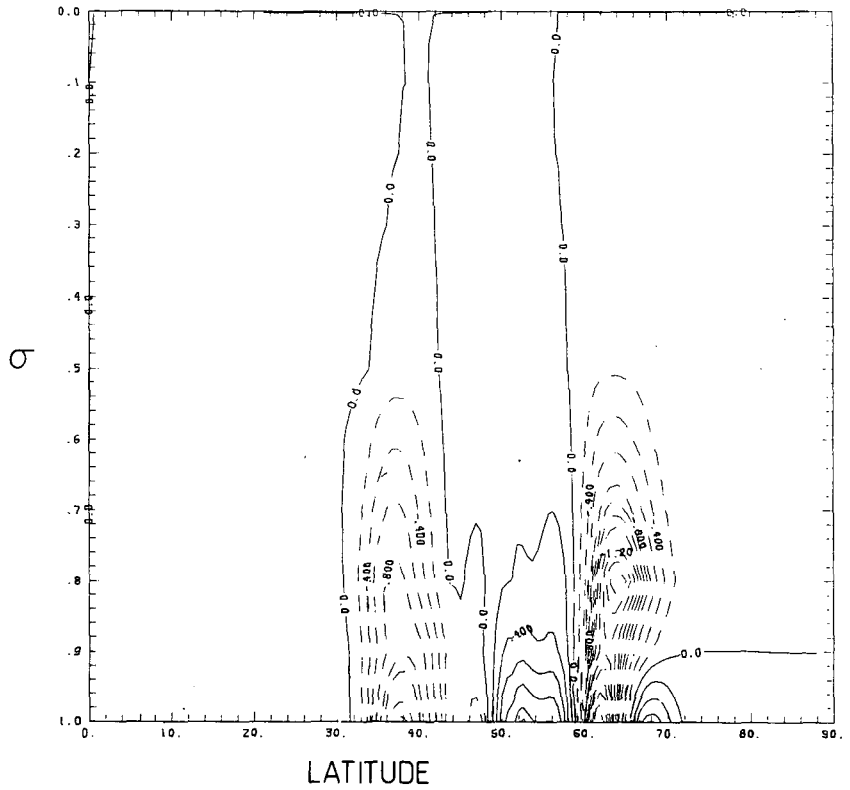

FIG. 12. Zonally averaged momentum flux $\overline{uv}$ for the disturbance shown in Fig. 11a.

sphere fluxes for March–May given in Fig. 4.9 of Newell *et al.* (1972), we see that again there are significant contributions to the poleward momentum flux in the latitude band between 10 and 50° and as well a region of equatorward flux centered on 70° latitude. One might speculate that modes like B at $m = 10$ and A at $m = 7$, when taken into the nonlinear regime, would contribute to the observed fluxes.

c. Eddy heat fluxes

Again, the eddy heat fluxes are centered at the same latitudes as the corresponding disturbance streamfunctions and are quite shallow like that shown in Fig. 9; the penetration of the heat fluxes into the middle atmosphere, of course, is greater for the longer waves than for the shorter waves. Thus modes A discussed above have heat fluxes centered near 70° latitude, while for mode B at $m = 10$ they are centered at 45° latitude.

By examining the eddy heat fluxes for March–May in Table 7.2 of Newell *et al.* (1974), we see that the maximum observed poleward fluxes occur at the same latitudes as for modes B.

8. Discussion and conclusions

The present study of the instability of Southern Hemisphere zonal flows for different months indicates that the growing perturbation modes may exhibit considerably more complicated behavior than found previously with idealized single jet basic states and with Northern Hemisphere zonal flows. For May and August, this is related to the presence of two jets, the subtropical and polar, whose relative importance in determining the growth rate and where the modes will grow depends on the zonal wavenumber. The fastest growing and shorter waves may grow either on the subtropical or polar jet while the longer waves usually occur close to the pole, even for January. Because of this, the meridional spread at the upper levels may sometimes be larger for the fastest growing modes than for the slower growing longer waves, in contrast to cases studied with idealized jets. For January, westward as well as the usual eastward-propagating modes exist, the former propagating in the westward wind near the polar regions in the lower troposphere and in the stratosphere.

The fastest and second-fastest growing modes at a given zonal wavenumber, whose structures have been analyzed, exhibit many properties in common with those previously studied with idealized single jet and Northern Hemisphere zonal flows. For example, the disturbance streamfunctions show a slight westward tilt with height and for some of the modes the qualitative nature of the streamfunctions and the zonally averaged momentum and heat fluxes is very similar to that found previously. In particular, the vertical structure problem of linear theory occurs, *viz.*, the amplitudes of streamfunctions, momentum and heat fluxes are too large at the surface compared with at the tropopause in relation to observations. Nevertheless, appropriate growing modes obtained with linear theory do have maximum streamfunction amplitude and eddy fluxes at the correct latitudes.

On the other hand, the growth rate and phase speed curves for May and August, in particular, are considerably more complicated than in previous studies. For August, the fastest and second-fastest growing modes with zonal wavenumber $m = 8$ have practically identical growth rates and similar phase speeds while the fastest growing mode, taken over all zonal wavenumbers considered, ocurs at $m = 16$, the largest wavenumber examined. For January and May, the growth rate maxima occur at an intermediate zonal wavenumber ($m = 10$) and these modes are propagating eastward. However, for January the fastest growing long waves ($m = 1$ to 5) are westward propagating.

For May the fastest growing mode (A) at $m = 10$ has considerably larger growth rate than for January and August. It has maximum amplitude at 70° latitude and a secondary maximum near 40° latitude and does not appear, on comparison with observations, to correspond to the most meteorologically significant mode. It also has associated with it a momentum flux (which is considerably more complicated than those studied previously) and a heat flux both of which do not occur at the latitudes of maximum observed fluxes. Instead, the second fastest growing mode (B) at $m = 10$ has streamfunction, momentum and heat fluxes whose maximum amplitudes occur at latitudes consistent with observations. It is argued that since the scale of A at $m = 10$ is small compared with B, the inclusion of viscosity could severely damp the growth of A and interchange the roles of A and B. These results, nevertheless, emphasize the importance of obtaining the complete growth rate spectrum, as given by the present eigenvalue method.

In a sequel to this work (Frederiksen, 1981), we analyze how viscosity and as well nonlinear, nongeostrophic and topographic effects may modify the results of linear instability theory.

Acknowledgments. It is a pleasure to thank W. Bourke for making available the basic fields used in this study. I am grateful to H. Rabich for assistance with developing contour plotting routines and to P. Nelson for drawing the graphs. I wish to thank P. D. Thompson and H. van Loon for comments on this article and A. Modahl for typing the manuscript.

REFERENCES

Baines, P. G., and J. S. Frederiksen, 1978: Baroclinic instability on a sphere in two-layer models. *Quart. J. Roy. Meteor. Soc.*, **104,** 45–68.

Blackmon, M. L., J. M. Wallace, N. Lau and S. L. Mullen, 1977: An observational study of the Northern Hemisphere wintertime circulation. *J. Atmos. Sci.*, **34,** 1040–1053.

Bourke, W., B. McAvaney, K. Puri and R. Thurling, 1977: Global modeling of atmospheric flow by spectral methods. *Methods Comput. Phys.*, **17,** 267–324.

Charney, J. G., 1947: The dynamics of long waves in a baroclinic westerly current. *J. Meteor.*, **4,** 135–162.

Eady, E. T., 1949: Long waves and cyclone waves. *Tellus*, **1,** 33–52.

Frederiksen, J. S., 1978a: Instability of planetary waves and zonal flows in two-layer models on a sphere. *Quart. J. Roy. Meteor. Soc.*, **104,** 841–872.

——, 1978b: Growth rates and phase speeds of baroclinic waves in multi-level models on a sphere. *J. Atmos. Sci.*, **35,** 1816–1826.

——, 1979a: The effect of long planetary waves on the regions of cyclogenesis: linear theory. *J. Atmos. Sci.*, **36,** 195–204.

——, 1979b: Baroclinic instability of zonal flows and planetary waves in multi-level models on a sphere. *J. Atmos. Sci.*, **36,** 2320–2335.

——, 1980: Zonal and meridional variations of eddy fluxes induced by long planetary waves. *Quart. J. Roy. Meteor. Soc.*, **106,** 63–84.

——, 1981: Growth and vacillation cycles of disturbances in Southern Hemisphere flows. *J. Atmos. Sci.*, **38** (in press).

——, and B. L. Sawford, 1980: Statistical dynamics of two-dimensional inviscid flow on a sphere. *J. Atmos. Sci.*, **37,** 717–732.

Gall, R., 1976a: A comparison of linear baroclinic instability theory with the eddy statistics of a general circulation model. *J. Atmos. Sci.*, **33,** 349–373.

——, 1976b: The effects of released latent heat in growing baroclinic waves. *J. Atmos. Sci.*, **33,** 1686–1701.

Green, J. S. A., 1970: Transfer properties of large-scale eddies and the general circulation of the atmosphere. *Quart. J. Roy. Meteor. Soc.*, **96,** 157–184.

Hartmann, D. L., 1979: Baroclinic instability of realistic zonal-mean states to planetary waves. *J. Atmos. Sci.*, **36,** 2336–2349 .

Knittel, J., 1976: Ein Beitrag zur Klimatologie der Stratosphäre der Südhalbkugel. *Meteor. Abhand.*, Ser. A, *Monogr.*, Band 2, Heft 1.

Lorenz, E. N., 1960: Energy and numerical weather prediction. *Tellus*, **12,** 364–373.

Newell, R. E., J. W. Kidson, D. G. Vincent and G. J. Boer, 1972: *The General Circulation of the Tropical Atmosphere and Interactions with Extratropical Latitudes,* Vol. 1. The MIT Press, 258 pp.

——, ——, —— and ——, 1974: *The General Circulation of the Tropical Atmosphere, and Interactions with Extratropical Latitudes,* Vol. 2. The MIT Press, 371 pp.

Simmons, A. J., and B. J. Hoskins, 1976: Baroclinic instability on the sphere: normal modes of the primitive and quasi-geostrophic equations. *J. Atmos. Sci.*, **33,** 1454–1477.

——, and ——, 1977: Baroclinic instability on the sphere: solutions with a more realistic tropopause. *J. Atmos. Sci.*, **34,** 581–588.

——, and ——, 1978: The life cycles of some nonlinear baroclinic waves. *J. Atmos. Sci.*, **35,** 414–432.

Stone, P. H., 1969: The meridional structure of baroclinic waves. *J. Atmos. Sci.*, **26,** 376–389.

van Loon, H., 1980: Transfer of sensible heat by transient eddies on the Southern Hemisphere: An appraisal of the data before and during FGGE. *Mon. Wea. Rev.*, **108,** 1774–1781.